Potential Sources of Decadal Climate Variability over Southern Africa

YUSHI MORIOKA

Application Laboratory, Japan Agency for Marine-Earth Science and Technology, Yokohama, Japan

FRANCOIS ENGELBRECHT

Climate Studies, Modelling and Environmental Health, Natural Resources and the Environment, Council for Scientific and Industrial Research, Pretoria, South Africa

SWADHIN K. BEHERA

Application Laboratory, Japan Agency for Marine-Earth Science and Technology, Yokohama, Japan

(Manuscript received 14 March 2015, in final form 6 August 2015)

ABSTRACT

Potential sources of decadal climate variability over southern Africa are examined by conducting in-depth analysis of available datasets and coupled general circulation model (CGCM) experiments. The observational data in recent decades show a bidecadal variability noticeable in the southern African rainfall with its positive phase of peak during 1999/2000. It is found that the rainfall variability is related to anomalous moisture advection from the southwestern Indian Ocean, where the anomalous sea level pressure (SLP) develops. The SLP anomaly is accompanied by anomalous sea surface temperature (SST). Both SLP and SST anomalies slowly propagate eastward from the South Atlantic to the southwestern Indian Ocean. The analysis of mixed layer temperature tendency reveals that the SST anomaly in the southwestern Indian Ocean is mainly due to eastward advection of the SST anomaly by the Antarctic Circumpolar Current. The eastward propagation of SLP and SST anomalies are also confirmed in the 270-yr outputs of the CGCM control experiment. However, in a sensitivity experiment where the SST anomalies in the South Atlantic are suppressed by the model climatology, the eastward propagation of the SLP anomaly from the South Atlantic disappears. These results suggest that the local air–sea coupling in the South Atlantic may be important for the eastward propagation of the SLP anomaly from the South Atlantic to the southwestern Indian Ocean. Although remote influences from the tropical Pacific and Antarctica were widely discussed, this study provides new evidence for the potential role of local air–sea coupling in the South Atlantic for the decadal climate variability over southern Africa.

1. Introduction

Climate variability at a decadal or longer time scale is a key issue for the society to mitigate climate-related risks and establish long-term adaptation plans for agriculture, fisheries, water management, city design, etc. A growing number of studies have to date elaborated on decadal or multidecadal climate variability, mainly in the Northern Hemisphere [e.g., Pacific decadal variability (Mantua et al. 1997) and Atlantic meridional oscillation (Schlesinger and Ramankutty 1994)], but few studies have attempted to examine the low-frequency variability in the Southern Hemisphere [e.g., South Atlantic (Venegas et al. 1997) and southern Indian Ocean (Allan et al. 1995)]. The relatively poor understanding of the low-frequency climate variability in the Southern Hemisphere may be at least partially attributed to a paucity of long-term reliable observations over the ocean. In fact, the total number of oceanic observations including ship and other marine in situ platforms is extremely small over the middle-to-high-latitude ocean before the 1980s (Fig. 1).

However, some land-based station data provide much evidence of the existence of decadal climate variability over southern Africa. For example, 18–20- and 10–12-yr oscillations are noticeable in the long-term rainfall data over South Africa (Tyson et al. 1975; Jury 2015). In

Corresponding author address: Dr. Yushi Morioka, Application Laboratory, JAMSTEC, 3173-25, Showamachi, Kanazawa-ku, Yokohama City, Kanagawa, 236-0001, Japan.
E-mail: morioka@jamstec.go.jp

DOI: 10.1175/JCLI-D-15-0201.1

© 2015 American Meteorological Society

Unauthenticated | Downloaded 05/18/25 08:50 PM UTC

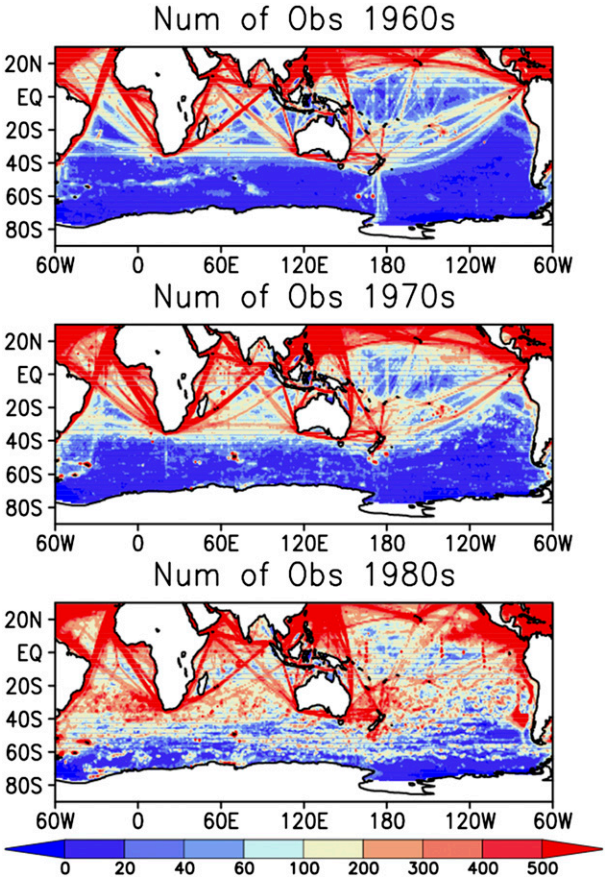

FIG. 1. Total number of oceanic observation for each decade.

particular, the 18–20-yr oscillation is significant in the northeastern part of the country. The 18–20-yr cycle is also detected in the rainfall data over the neighboring countries such as Zimbabwe (Ngara et al. 1983) and Botswana (Jury et al. 1992). This suggests the possible existence of 18–20-yr cycle in the rainfall variability over the larger southern African region.

The physical mechanisms underlying the 18–20-yr oscillation in rainfall variability have been intensely discussed with respect to remote influences from outside southern Africa. In particular, a major contribution to this variability is considered to be the atmospheric standing wave 1 (Tyson 1986), which may in turn respond to a low-frequency variability in the sea surface temperature (SST) over the eastern equatorial Pacific (Mason and Jury 1997; Reason and Rouault 2002). Since the interannual climate variability in the tropical Pacific in relation to El Niño–Southern Oscillation (ENSO) can significantly influence southern African rainfall through atmospheric teleconnection (Mason 1990), a low-frequency modulation of tropical Pacific variability may contribute to the 18–20-yr cycle in the southern African rainfall. Besides the climate variability in the tropical Pacific, a remote influence from the atmospheric variability in high latitudes on southern African rainfall was recently proposed by Malherbe et al. (2014). They provided new evidence that the bidecadal rainfall variability in South Africa might have a relation with low-frequency variability of the southern annular mode (SAM; Thompson and Wallace 2000) and an associated deep anticyclonic anomaly over the southwestern Indian Ocean.

Local influences from climate variability over the southern Indian and South Atlantic Oceans can be also important, because of the proximity to southern Africa. The dominant high pressure system over the southern Indian Ocean (i.e., the Mascarene high) underwent significant multidecadal variability during the last century (Allan et al. 1995) and affected the SST variability in the southern Indian Ocean at multidecadal time scales (Reason et al. 1996). The multidecadal SST variability in the southern Indian Ocean, in turn, could influence the overlying atmospheric circulation and, hence, the southern African rainfall at multidecadal time scales, as suggested by several model studies (Reason et al. 1998; Reason and Godfred-Spenning 1998). Since the Mascarene high plays an important role in the southern African rainfall through moisture advection (e.g., Engelbrecht et al. 2009), a low-frequency variability in the Mascarene high can influence the rainfall variability.

On the other hand, the South Atlantic experiences a 14–16-yr cycle with respect to the sea level pressure (SLP) and SST anomalies (Venegas et al. 1997). In particular, the SST in the midlatitudes of the South Atlantic shows a clear interdecadal variability, which is strongly connected to anomalous atmospheric circulation (Colberg and Reason 2007). A model study by Reason and Murray (2001) also suggested that SST anomalies stretching zonally over the South Atlantic and the southern Indian Oceans may induce anomalous atmospheric circulation over southern Africa by modifying the location and intensity of storm tracks in the midlatitudes. However, a potential influence of the South Atlantic SST on the low-frequency climate variability over southern Africa has yet to be identified.

In this historical context, this study aims to more completely describe low-frequency climate variability over southern Africa and identify its potential causes, with emphasis on a role of the local SST variability in the South Atlantic. Section 2 provides descriptions of the data, model, and methodology. Section 3 provides observational evidence for the decadal climate variability over southern Africa in recent decades, and proposes a possible physical mechanism driving the low-frequency variability. The observed physical mechanism is then

Unauthenticated | Downloaded 05/18/25 08:50 PM UTC

further explored in section 4 by performing coupled general circulation model (CGCM) experiments. Finally, section 5 summarizes all the results obtained in this study and discusses their significance in the historical context of decadal climate variability studies.

2. Data, model, and methodology

a. Data and reanalysis

For the analysis of historical atmospheric variability, monthly mean ERA-Interim data (Dee et al. 2011) provided by the European Centre for Medium-Range Weather Forecasts (ECMWF) is used. The spatial resolution is a spectral T255 (~80 km) on 60 levels in the vertical, but the outputs were extrapolated onto a 1° × 1° resolution horizontal grid to match the horizontal resolution of the ocean datasets. The analysis period is the recent decades since 1982 when the satellite data was fully incorporated into the reanalysis. Though the data period appears to be somewhat short for an analysis of decadal climate variability, similar decadal variability as found in this paper has been documented by Malherbe et al. (2014) using different datasets. This suggests that our results are quite robust irrespective of data sources. For comparison with other reanalysis, Japanese 55-year Reanalysis Project (JRA-55; Ebita et al. 2011) provided by Japan Meteorological Agency and the National Centers for Environmental Prediction–U.S. Department of Energy (NCEP–DOE) Atmospheric Model Intercomparison Project phase II (AMIP-II) reanalysis (NCEP2; Kanamitsu et al. 2002) were used. However, the results are qualitatively the same as those from the ERA-Interim (figure not shown). For the precipitation, the Global Precipitation Climatology Project (GPCP), version 2, precipitation dataset (Adler et al. 2003), which has a horizontal resolution of 2.5° × 2.5°, is used. Other land surface rainfall datasets provided by the Climatic Research Unit (CRU; Harris et al. 2014) and the Global Precipitation Climatology Centre (GPCC; Schneider et al. 2011) were also analyzed over the same period for comparison, but yielded very similar results in terms of low-frequency variability in southern African rainfall (figure not shown).

For the oceanic datasets, monthly mean optimum interpolation SST (OISST; Reynolds et al. 2002), which has a horizontal resolution of 1° × 1°, is analyzed. Also, the monthly numbers of oceanic observations are derived from the International Comprehensive Ocean–Atmosphere Data Set (ICOADS) 1° enhanced products, provided by the NOAA/ESRL/Physical Sciences Division (2011). For the other oceanic variables in the subsurface ocean, monthly mean outputs of the Ocean Reanalysis System 4 (ORAS4; Balmaseda et al. 2013) provided by the ECMWF are used. The availability of the ocean reanalysis limits the analysis period to 1982–2009. For all the above data and reanalysis, monthly anomalies were calculated with respect to the monthly climatology, after removing the linear monthly trends by using a least squares method.

TABLE 1. CGCM experiments conducted in the present study.

	SST-nudging area	Analysis period
CTR	None	270 yr
SAO	South Atlantic (10°–55°S)	270 yr

b. Coupled general circulation model

For the CGCM, the Scale Interaction Experiment–Frontier Research Center for Global Change (FRCGC) model, version 2 (SINTEX-F2; Masson et al. 2012), which is an upgraded version of SINTEX-F1 (Luo et al. 2003, 2005), is used. The atmospheric component is based on ECHAM5 (Roeckner et al. 2003), which was originally developed at ECMWF and has a parameterization package developed by the Max Planck Institute for Meteorology in Hamburg, Germany. The ECHAM5 has 31 levels in the vertical on a Gaussian grid of T106 spectral truncation. The oceanic component is Nucleus for European Modelling of the Ocean (NEMO; Madec 2008), which includes the Louvain-la-Neuve Sea Ice Model 2 (LIM2; Fichefet and Maqueda 1997) and has 0.5° × 0.5° horizontal resolution of ORCA configuration (ORCA05) with 31 levels in the vertical. The atmospheric and oceanic fields are exchanged every 2 h with no flux correction by means of the Ocean Atmosphere Sea Ice Soil, version 3 (OASIS3) coupler (Valcke et al. 2004). For the control run (CTR) experiment, the SINTEX-F2 was integrated for 300 yr, and monthly mean outputs from the last 270 yr are analyzed considering the oceanic adjustment to the interannually varying atmospheric forcing.

To examine the possible impact from SST anomalies in the South Atlantic on the low-frequency climate variability over southern Africa, another CGCM experiment [i.e., the South Atlantic Ocean (SAO) experiment] was performed (Table 1). In the SAO experiment, SST in the South Atlantic (55°–10°S, 60°W–20°E) is nudged to the monthly climatology of the CTR experiment. A strong negative feedback ($-9600\,\mathrm{W\,m^{-2}\,K^{-1}}$) is applied to the surface heat flux so that the temperature in the upper 200 m, a typical maximum in the mixed layer depth in midlatitudes, is restored within 1 day. The SAO experiment was integrated for 300 yr, and the monthly outputs for the last 270 yr are used for the present analysis to match with the CTR experiment.

Unauthenticated | Downloaded 05/18/25 08:50 PM UTC

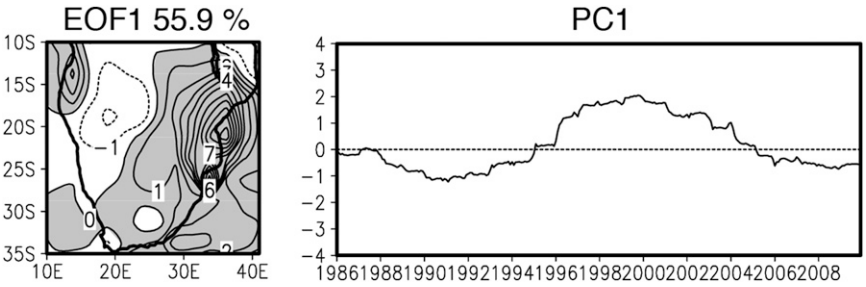

FIG. 2. (left) Spatial pattern of the first EOF mode of the 8-yr running mean rainfall anomaly (mm month^{-1}). The percentage above the left panel shows the fraction of total variance explained by the first EOF mode. (right) Time series of the principal component of the first EOF mode. The time series is normalized by the standard deviation.

c. *Diagnosis on mixed layer temperature variations*

To quantitatively examine the low-frequency SST variability, the tendency anomaly in the mixed layer temperature T_m at each grid is estimated by using

$$\delta\left(\frac{\partial T_m}{\partial t}\right) = \delta\left(\frac{Q_{\text{net}} - q_d}{\rho c_p H}\right) - \delta(\mathbf{u}_m \cdot \nabla T_m) - \delta\left(\frac{\Delta T}{H} w_e\right) + \text{Res} \quad (1)$$

(Qiu and Kelly 1993; Moisan and Niiler 1998). Here, $\delta(\,)$ is a deviation from the monthly climatology. The first term on the right-hand side of Eq. (1) indicates the contribution from the net surface heat flux, where Q_{net} is the net surface heat flux, q_d is the downward solar insolation penetrating through the mixed layer bottom (Paulson and Simpson 1977), ρ ($=1027\,\text{kg m}^{-3}$) is the density of the seawater, c_p ($=4187\,\text{J kg}^{-1}\,\text{K}^{-1}$) is the specific heat of the seawater, and H is the surface mixed layer depth defined as the depth at which temperature becomes lower by 0.5°C compared to the SST. The second term on the right-hand side of Eq. (1) shows the contribution from the horizontal advection, where $\mathbf{u}_m$ is the horizontal velocity vertically averaged in the surface mixed layer. The third term represents the contribution from the entrainment, where ΔT ($\equiv T_m - T_{-H-20\text{m}}$) is the temperature difference between the surface mixed layer and the entrained water. We use the water temperature at 20 m below the mixed layer base as the temperature of the entrained water (Yasuda et al. 2000). Also, w_e [$\equiv \partial H/\partial t + \nabla \cdot (\mathbf{u}_m H)$] is the entrainment velocity and it is assumed to vanish when it becomes negative (Kraus and Turner 1967). The residual term Res comprises other oceanic physical processes such as diffusion and detrainment.

3. Observational evidence

For description of low-frequency climate variability over southern Africa, 8-yr running means are first applied to monthly anomalies in the observational data and reanalysis. The selection of an 8-yr running mean period is due to the short record of observational data, and to remove the influence of the dominant interannual climate variability associated with ENSO. The results are found not to qualitatively differ from those obtained with other running mean periods such as 9 or 10 yr.

Figure 2 shows a spatial pattern and its associated time series of the dominant rainfall variability over southern Africa, which was derived from the empirical orthogonal function (EOF) analysis. The rainfall variability represents positive (negative) values in the southeastern (southwestern) part of southern Africa with its positive phase of peak during 1999/2000. This pattern explains more than half of the rainfall variability at 55.9%, significantly separated from the second EOF mode (North et al. 1982). The time series clearly shows a bidecadal variability with a frequency of 18–20 yr, which was already reported in the previous studies (Tyson et al. 1975; Ngara et al. 1983; Jury et al. 1992; Malherbe et al. 2012). The positive peak of a bidecadal oscillation in 1999/2000 is also observed in a recent study by Jury (2015), although there are some differences in the analysis period and the study region (see his Fig. 2a).

Climatologically, southern African rainfall undergoes a strong seasonal variation and reaches its peak during the austral summer (December–February) under the strong influence of the South Indian convergence zone (Cook 2000). Considering the peak rainfall season, the 8-yr moving average of December–February rainfall anomalies centered on December 1999–February 2000 is shown in Fig. 3a. It should be noted that the negative rainfall peak during December 1990–February 1991 is found to show almost the opposite spatial pattern in rainfall anomalies than for the case of the positive rainfall peak (figure not shown). Consistent with the spatial pattern derived from the EOF analysis, the above-normal rainfall is observed over the southeastern part of southern Africa extending toward the Mozambique Channel. To examine

Unauthenticated | Downloaded 05/18/25 08:50 PM UTC

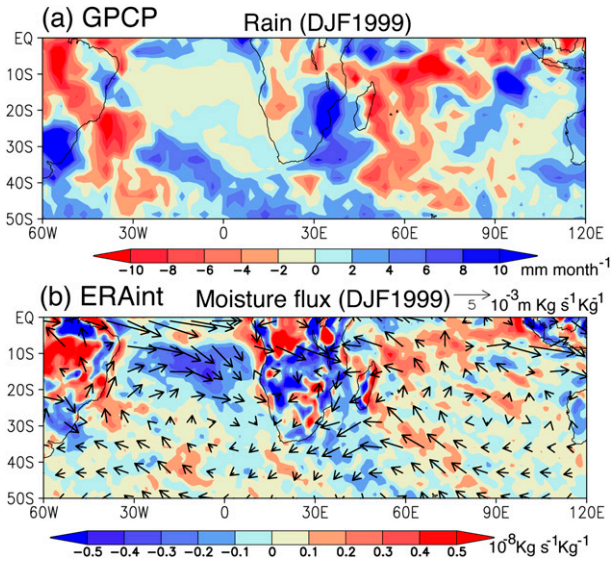

FIG. 3. (a) The 8-yr running mean rainfall anomaly observed during December 1999–February 2000. (b) As in (a), but for the moisture flux anomaly (arrows) and its divergence (color shading) at 850 hPa.

potential sources of low-frequency rainfall variability, the 8-yr moving averages of the December–February moisture flux anomaly and its divergence at 850 hPa centered on December 1999–February 2000 are calculated in Fig. 3b. The moisture flux anomaly represents anomalous convergence over southern Africa and the Mozambique Channel, which is associated with the anomalous moisture advection from the southwestern Indian Ocean. This mainly contributes to the rainfall increase over the southeastern part of southern Africa. However, there are also some regions with rainfall increase over southeastern Africa where the moisture flux shows a divergent anomaly. These are located near the west of the steep escarpment of the southeastern part of southern Africa.

The moisture flux anomalies associated with wet periods over the southeastern part of southern Africa occur in strong relation with certain patterns of atmospheric variability. Figures 4a and 4b show anomalies of SLP and geopotential height at 250 hPa during December 1999–February 2000. The SLP anomaly shows anomalous high pressure over the southwestern Indian Ocean, which contributes to the advection of moisture toward the southeastern part of southern Africa (Fig. 4a). It is also associated with the positive geopotential height anomaly in the upper troposphere, representing a barotropic structure of the circulation anomalies (Fig. 4b). This result is fairly consistent with the atmospheric anomalies identified by Malherbe et al. (2014) to occur during 8-yr-long wet phases over the southeastern part of southern Africa. These atmospheric anomalies appear to be closely related to an upstream wave train of positive and negative anomalies in the South Atlantic (Fig. 4b). Also, another wave train is evident in the South Pacific, where the positive anomaly over New Zealand and the negative anomaly in high latitudes compose the Pacific–South American teleconnection pattern (Mo and Paegle 2001). In fact, the rainfall anomaly shows a remarkable negative amplitude in the central-western tropical Pacific (Fig. 4c), which is associated with the negative geopotential height anomaly (i.e., anomalous wind convergence) in the upper

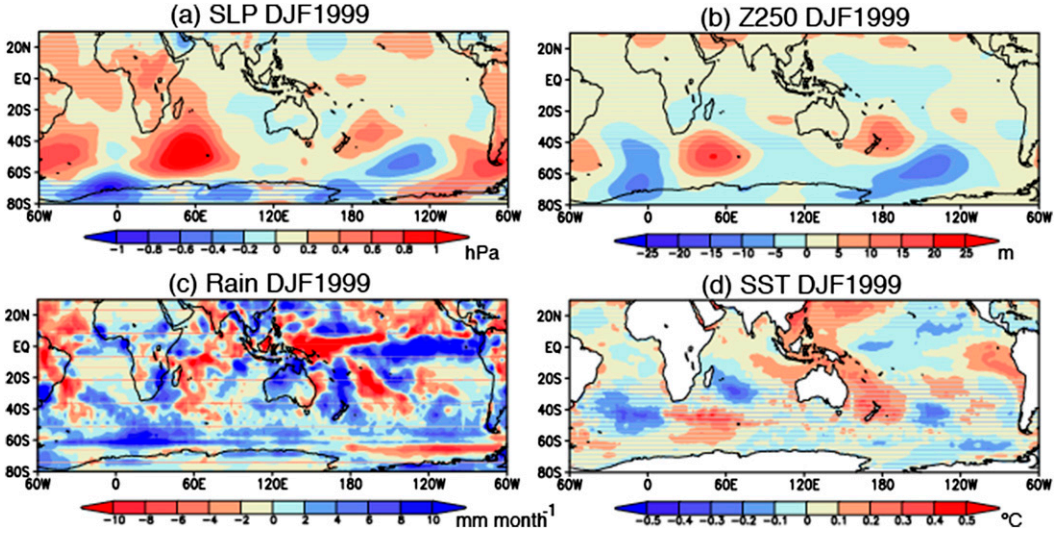

FIG. 4. (a) The 8-yr running mean SLP anomaly during December 1999–February 2000. (b)–(d) As in (a), but for the anomalies of geopotential height at 250 hPa, rainfall, and SST, respectively.

Unauthenticated | Downloaded 05/18/25 08:50 PM UTC

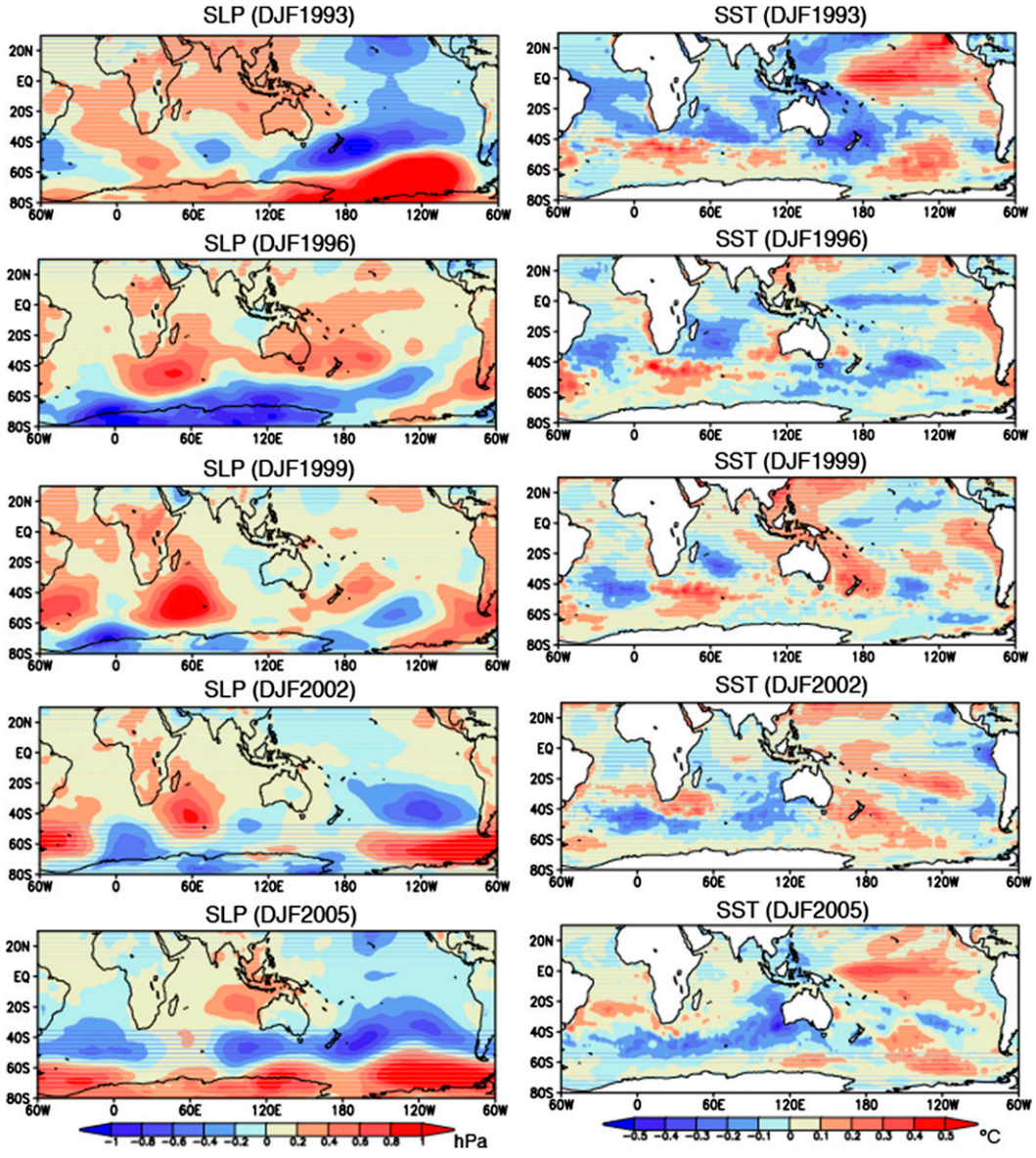

FIG. 5. (left) Time evolution of 8-yr running mean SLP anomaly with 3-yr interval (top)–(bottom) from December 1993–February 1994 through December 2005–February 2006. (right) As in (left), but for the SST anomaly.

troposphere (Fig. 4b). The rainfall decrease appears to be linked with the cold SST anomaly in the central tropical Pacific (Fig. 4d), which is flanked with the warm SST anomalies in the western and eastern tropical Pacific, representing the negative phase of El Niño Modoki (Ashok et al. 2007) (i.e., La Niña Modoki). As such, the atmospheric teleconnection from the tropical Pacific can be one of sources of the SLP variability in the southwestern Indian Ocean (Malherbe et al. 2014).

The possible link with the low-frequency variability in the tropical Pacific is also found in time evolutions of SLP and SST anomalies (Fig. 5). During December 1993–February 1994, the SST anomaly shows the warm peak in the central tropical Pacific with the cold anomaly to the west, representing warm phase of the interdecadal Pacific oscillation (IPO; Power et al. 1999). It turns into La Niña Modoki during December 1999–February 2000 and returns again to warm phase of the IPO during December 2005–February 2006. However, the relatively short analysis period makes it difficult to conclusively demonstrate a link to El Niño Modoki or the IPO. Moreover, the SST and SLP anomalies in the southwestern Indian Ocean develop rather slowly compared to the variability in the tropical Pacific. This indicates that there exist other remote and/or local factors driving the SLP and SST anomalies in the southwestern Indian Ocean. In fact, both SLP and SST

Unauthenticated | Downloaded 05/18/25 08:50 PM UTC

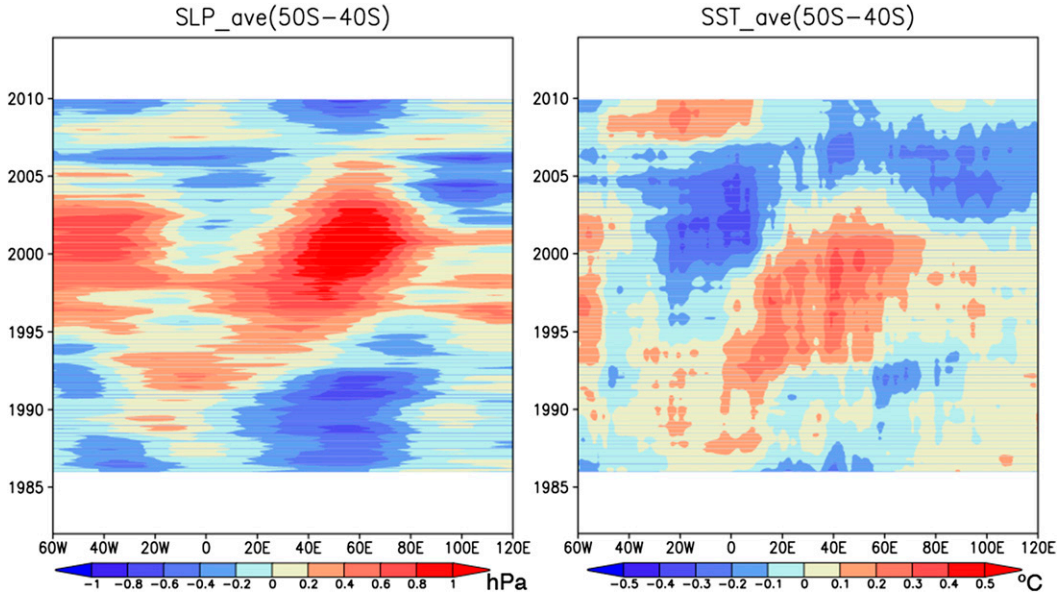

FIG. 6. (left) Time evolution of 8-yr running mean SLP anomaly averaged between 50° and 40°S as a function of longitude. (right) As in (left), but for the SST anomaly.

anomalies slowly propagate eastward from the South Atlantic to the southwestern Indian Ocean.

The eastward propagation of SST and SLP anomalies between the South Atlantic and southern Indian Oceans are evident in time–longitude sections of anomalies averaged between 50° and 40°S (Fig. 6). The peaks of SLP and SST anomalies appear between 40° and 60°E in 2000, and can be traced back to the anomalies between 20°W and 0° in the early 1990s, representing a clear eastward propagation from the South Atlantic. By applying the least squares method to the dominant SST anomalies between 20°W and 60°E, the propagation speed of the SST anomalies is estimated to be approximately 1.5 cm s^{-1}, relatively slow compared to the speed of mean eastward-flowing Antarctic Circumpolar Current (ACC) of 5–10 cm s^{-1}.

To quantitatively check a potential role of oceanic currents in the eastward propagation of SST anomalies, a tendency anomaly of the mixed layer temperature in the southwestern Indian Ocean (50°–40°S, 40°–60°E) is calculated by using the ORAS4. The SST anomaly derived from the ORAS4 during December 1999–February 2000, when the warm SST anomaly peaks in the southwestern Indian Ocean, is spatially consistent with the observed SST anomaly in the OISST (Fig. 7). In the southwestern Indian Ocean, the tendency anomaly of the mixed layer temperature is found to be positive before 2000, where afterward it becomes negative (Fig. 8a). Although there is a positive contribution from the meridional advection in the early 1990s and also from the surface heat flux in the late 1990s, it is the zonal advection that mainly contributes to the positive tendency anomaly in the mixed layer temperature. In particular, the anomalous contribution from the zonal advection is mainly due to the advection of the mixed layer temperature anomaly by the mean zonal current (Fig. 8b). In the southwestern Indian Ocean (50°–40°S, 40°–60°E), where the mixed layer temperature balance is examined, the ACC

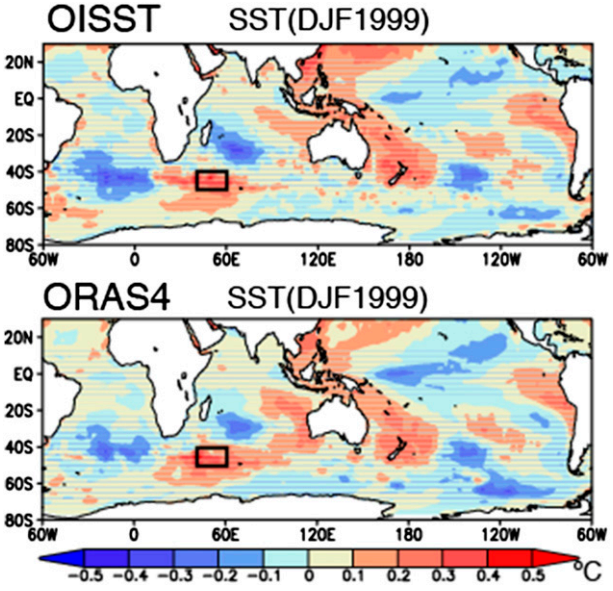

FIG. 7. (top) The 8-yr running mean SST anomaly observed during December 1999–February 2000. (bottom) As in (top), but for the SST anomaly reproduced by the ORAS4. The boxes indicate the region 50°–40°S, 40°–60°E where the observed SST anomaly shows its peak.

Unauthenticated | Downloaded 05/18/25 08:50 PM UTC

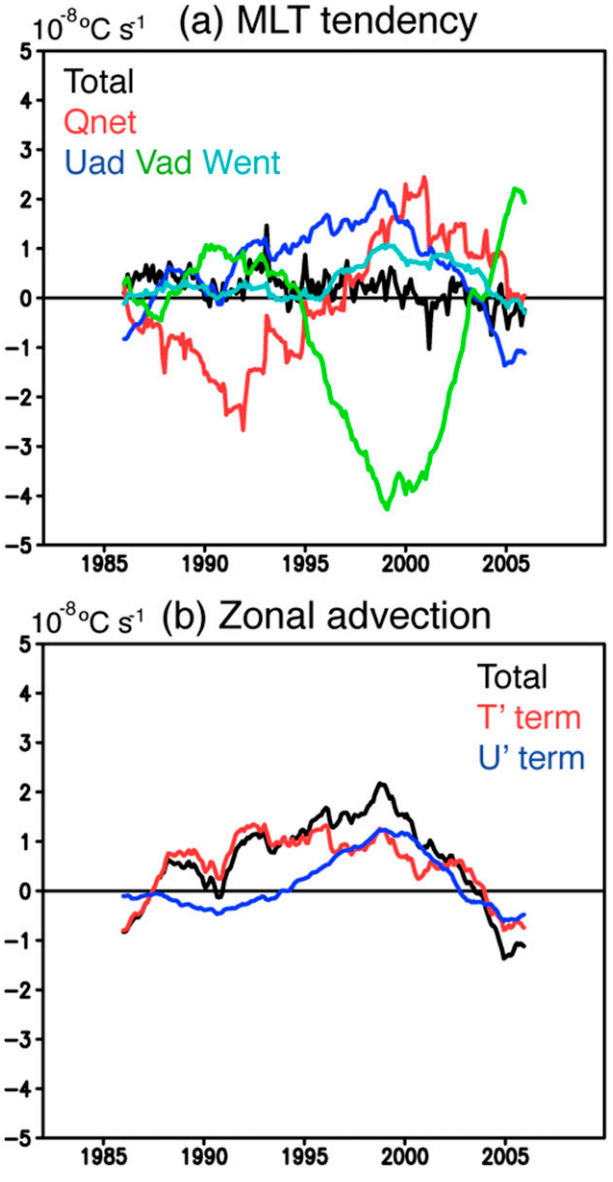

FIG. 8. (a) Time series of 8-yr running mean mixed layer temperature tendency anomaly averaged over the southwestern Indian Ocean (50°–40°S, 40°–60°E, the boxes in Fig. 7). The total tendency anomaly of mixed layer temperature (black line) and each contribution from the surface heat flux (red line), zonal advection (blue line), meridional advection (green line), and entrainment (light blue line) are shown. (b) As in (a), but for the contribution from the zonal advection. The total contribution from the zonal advection (black line) and each contribution from the mixed layer temperature anomaly (red line) and zonal velocity anomaly (blue line) are shown.

constantly flows eastward, interacting with the Agulhas Return Current from the north. Thus, the ACC appears to play an important role in advecting the SST anomalies from the South Atlantic toward the southwestern Indian Ocean.

4. CGCM experiments

The physical mechanism underlying the SST anomaly in the southwestern Indian Ocean is identified in the previous section, but the generation mechanism of the SLP anomaly remains unclear. As described in the reanalysis, both the local SST anomalies and the atmospheric teleconnection from outside the southern Indian Ocean may be crucial for the generation of SLP anomaly, but their relative contribution is not fully understood. Although potential roles of the atmospheric teleconnection from the tropical Pacific and the high latitudes were already discussed in the literature (Mason and Jury 1997; Reason and Rouault 2002; Malherbe et al. 2014), roles of local SST anomalies in the South Atlantic and southern Indian Ocean have yet to be identified. Considering the clear eastward propagation of the observed SLP and SST anomalies from the South Atlantic, the impacts of local SST anomalies, particularly in the South Atlantic, are worthy to be examined.

From this perspective, 270-yr outputs from the two types of CGCM experiments (i.e., the CTR and SAO experiments) are examined. The Fourier spectrum of all monthly SLP anomalies averaged in the southwestern Indian Ocean (50°–40°S, 40°–60°E) shows the significant peak at around 20 yr in the CTR experiment (Fig. 9a), consistent with the observed bidecadal variability in the southern African rainfall (Fig. 2). However, the simulated bidecadal peak disappears in the SAO experiment (Fig. 9a), rather shifts to a lower frequency at around 30 yr and a higher frequency at around 12 yr. The reduction in the bidecadal spectrum peak is also noticeable in the Fourier spectrum of the SST anomalies (Fig. 9b). The significant spectral peak at 25 yr in the CTR experiment disappears in the SAO experiment, and shifts to a higher frequency at around 12 yr. The remarkable differences in the Fourier spectrums between the two experiments suggest that the SST anomaly in the South Atlantic may be important for the SLP anomaly as well as the SST anomaly in the southwestern Indian Ocean at a bidecadal time scale.

To highlight the decadal variability in the SLP and SST anomalies in the CGCM experiments, the bandpass filter with a frequency period of 8–32 yr is applied to the monthly anomalies. This frequency band covers most of the decadal peaks simulated in the CTR experiment (Fig. 9). Figure 10 shows time series of the bandpass-filtered SLP and SST anomalies averaged in the southwestern Indian Ocean (50°–40°S, 40°–60°E). In both the CTR and SAO experiments, the SLP anomaly is mostly in phase with the SST anomaly, indicating existence of local air–sea coupling. The standard deviation of the SLP anomaly over the analysis period is 0.36 hPa in the

Unauthenticated | Downloaded 05/18/25 08:50 PM UTC

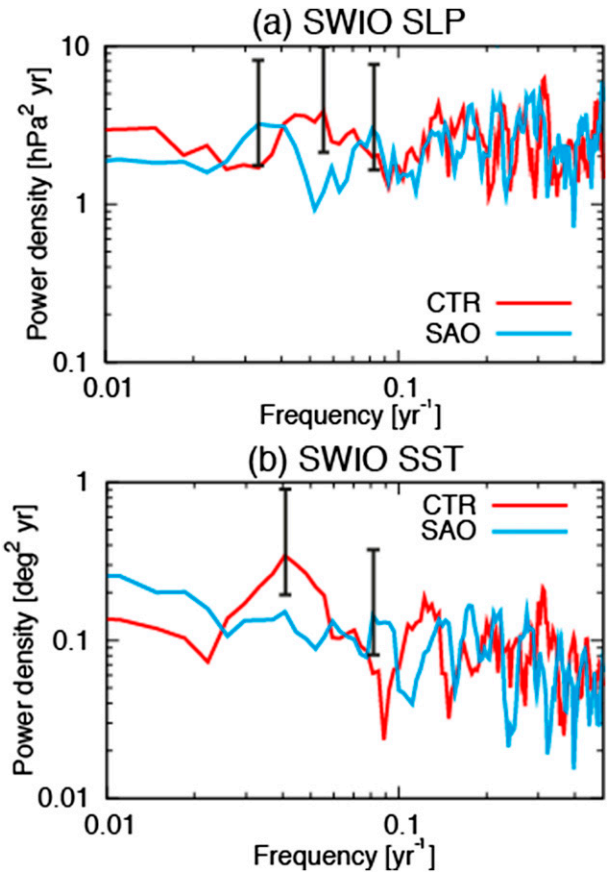

FIG. 9. (a) Fourier spectrum of SLP anomaly averaged over the southwestern Indian Ocean (50°–40°S, 40°–60°E). The CTR (red line) and SAO (light blue line) experiments are shown. (b) As in (a), but for the SST anomaly. Error bars indicate the 90% confidence level of spectral peaks estimated by Pearson's χ^2 test.

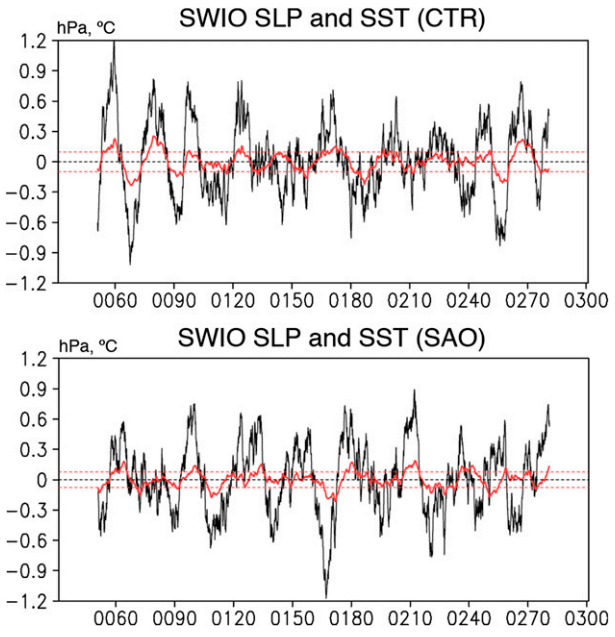

FIG. 10. (top) Time series of 8–32-yr bandpassed SLP (black line) and SST (red line) anomalies averaged over the southwestern Indian Ocean (50°–40°S, 40°–60°E) from the CTR experiment. The red dotted lines show plus and minus one standard deviation of the SST anomaly. (bottom) As in (top), but for the SLP and SST anomalies from the SAO experiment.

CTR experiment, almost the same as 0.35 hPa in the SAO experiment. On the other hand, the standard deviation of the SST anomaly is 0.1°C in the CTR experiment, but reduces by 20% to 0.08°C in the SAO experiment. Compared to the SLP anomaly, the SST anomaly in the southwestern Indian Ocean is influenced more by the SST anomaly in the South Atlantic.

To investigate a potential role of local SST anomaly in the SLP anomaly, composite analysis is conducted for the warm (cold) SST events when the time series of the SST anomaly during austral summer in the southwestern Indian Ocean exceeds the one (minus one) standard deviation (Fig. 10). This approach leads to six warm (cold) events in the CTR experiment and six warm (eight cold) events in the SAO experiment. Since results of the cold SST events are found to be nearly opposite of those of warm SST events, only the composite SLP and SST anomalies for the warm events are shown in Fig. 11. Note that Yr(0) indicates the year when the SST anomaly in the southwestern Indian Ocean reaches their peak in Fig. 10. The SLP anomaly in the CTR experiment represents anomalous high pressure developing in the southern Indian Ocean, which is associated with the warm SST anomaly as described in the reanalysis (Figs. 4a,d). The positive SLP anomaly extends farther east to the south of Australia and encircle a negative SLP anomaly over Antarctica. This seesaw SLP anomaly pattern comprises a positive phase of SAM (Thompson and Wallace 2000), indicating a possible link with the high-latitude atmospheric variability (Malherbe et al. 2014). On the other hand, in the SAO experiment, the possible link with the positive SAM is not visible, but in the southwestern Indian Ocean, the anomalous high pressure still appears in association with the warm SST anomaly. This suggests that there may exist a local influence from the SST anomaly in the southern Indian Ocean or remote influences besides the SAM.

To further examine the influence from the SST anomaly in the South Atlantic, time evolutions of composite SLP and SST anomalies averaged in 50°–40°S for the warm SST events are described in Fig. 12. As described in the observational data and reanalysis, the eastward propagation of SLP and SST anomalies from the South Atlantic is evident in the CTR experiment (Fig. 12a). The propagation speed is estimated approximately by 2.4 cm s^{-1}, slightly faster than that in the

Unauthenticated | Downloaded 05/18/25 08:50 PM UTC

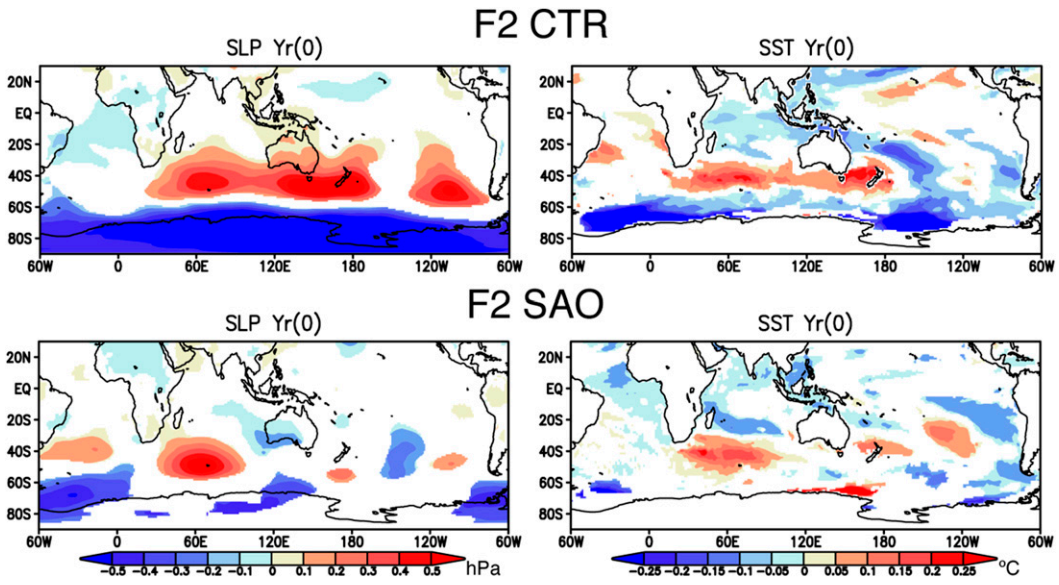

FIG. 11. (top) Composite of 8–32-yr bandpassed (left) SLP and (right) SST anomalies during austral summer of Yr(0) in the CTR experiment. (bottom) As in (top), but for the SAO experiment. Color shading indicates statistically significant anomalies exceeding the 90% confidence level of the two-tailed Student's *t* test.

observational results (Fig. 6). On the other hand, in the SAO experiment, the SLP anomaly appears to propagate both eastward and westward from 20°E between the South Atlantic and the southern Indian Oceans (i.e., the eastern boundary of the SST-nudging experiment; Fig. 12b). The difference in the propagation of SLP anomaly between the CTR and SAO experiments indicates that the local air–sea interaction in the South Atlantic plays an important role in generating the eastward propagation of the SLP anomalies from the South Atlantic.

SST anomalies in midlatitudes were considered to have weaker effects on the atmosphere than those in the tropics, but recently, a growing number of studies have reported that the midlatitude SST anomalies are able to affect the transient eddy activity through change in the near-surface baroclinicity and, hence, modulate the stationary eddies through scale interaction (Nakamura and Shimpo 2004; Nakamura 2012; Morioka et al. 2015). To investigate this local effect in a simple way, time evolution of composite anomalies of meridional SST gradient and zonal wind at 250 hPa is described in Fig. 13. It should be noted that composite anomalies averaged between 45° and 35°S are shown, because the warm SST anomaly peaks at around 45°S. North of the warm SST anomaly in the CTR experiment, the SST gradient anomalously weakens and the negative SST gradient anomaly slowly propagates eastward from the South Atlantic (Fig. 13a). Since the weakening of near-surface baroclinicity leads to weakening of transient eddies, the weaker SST gradient may be a favorable condition for sustaining the anomalous high pressure. In fact, in association with this weaker SST gradient, the zonal wind in the upper troposphere anomalously weakens, and the negative wind anomaly also slowly propagates from the South Atlantic (Fig. 13a). On the other hand, in the SAO experiment, the eastward propagation of the zonal wind anomaly from the South Atlantic is unclear (Fig. 13b). Rather, the propagation appears to start from the boundary at 20°E between the South Atlantic and southern Indian Oceans. This suggests that the SST anomaly in the South Atlantic may play some role in the overlying SLP anomaly through modulation of transient eddies associated with the meridional SST gradient change. The potential impact of the midlatitude SST anomalies on the transient eddy activity is also discussed in a model study by Reason and Murray (2001) with idealized SST anomalies stretching over the South Atlantic and the southern Indian Oceans.

Finally, the possible impact of these SST and SLP anomalies onto the southern African rainfall is evident from the model simulations. The composite rainfall anomaly during the austral summer of Yr(0) shows a slightly wetter condition over the southern Africa (Fig. 14a), which is associated with the anomalous moisture advection from the southwestern Indian Ocean (Fig. 14b). However, some regions over southern Africa show anomalous divergence of the moisture flux. Also, there is a distinct difference with the

Unauthenticated | Downloaded 05/18/25 08:50 PM UTC

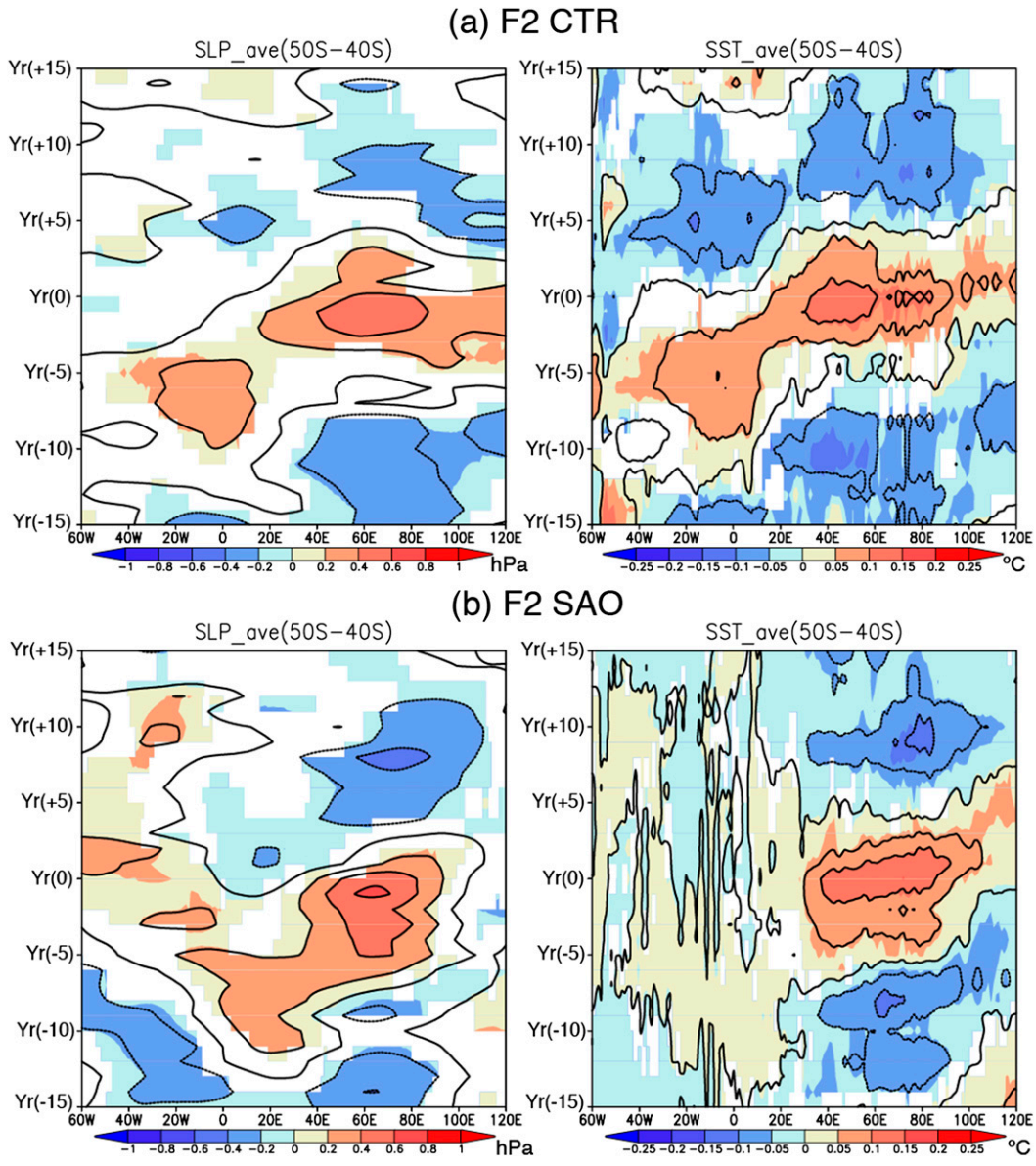

FIG. 12. (a) Time series of 8–32-yr bandpassed (left) SLP and (right) SST anomalies averaged between 50° and 40°S as a function of longitude. Composite anomalies for the positive events in the CTR experiment are shown. (b) As in (a), but for the SAO experiment. Color shading indicates significant anomalies exceeding the 90% confidence level of the two-tailed Student's *t* test.

observations, in which drier conditions prevail over Angola and Namibia (Fig. 3). These may be related to misrepresentation of atmospheric circulation and/or land surface process over southern Africa, which suggests the need for further studies using regional climate models.

5. Summary and discussion

By conducting data analysis and coupled general circulation model (CGCM) experiments, potential sources of decadal climate variability over southern Africa are described. During recent decades since 1982, southern African rainfall shows a distinct bidecadal variability (18–20-yr cycle) and, in its positive phase of peak during 1999/2000, the rainfall was above normal over the southeastern part of southern Africa. The development of the anomalous high pressure in the southwestern Indian Ocean helps advect more moisture toward southern Africa, contributing to the rainfall increase over southern Africa. The anomalous high pressure is found to slowly propagate eastward from the South Atlantic to

Unauthenticated | Downloaded 05/18/25 08:50 PM UTC

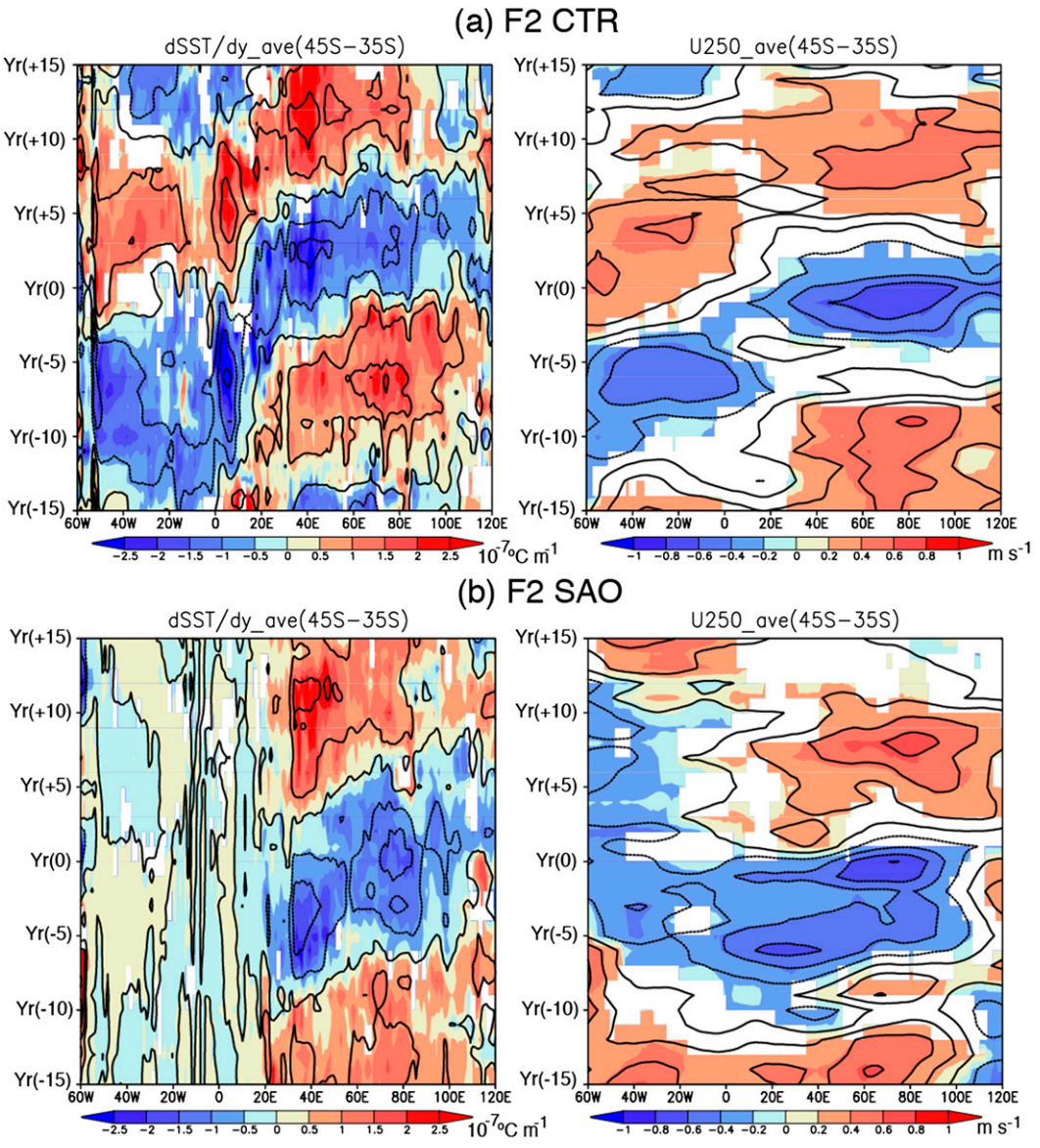

FIG. 13. As in Fig. 12, but for (left) the meridional SST gradient and (right) zonal wind at 250 hPa averaged between 45° and 35°S. Color shading indicates significant anomalies exceeding the 90% confidence level of the two-tailed Student's *t* test.

the southwestern Indian Ocean, in association with the warm SST anomaly. The mixed layer heat balance reveals that the warm SST anomaly is mainly advected by the eastward mean flow in the region (i.e., the Antarctic Circumpolar Current). The eastward propagation of SLP and SST anomalies are also confirmed in the 270-yr outputs of CGCM control experiment, but in the absence of the SST anomalies in the South Atlantic, the eastward propagation of the SLP anomaly from the South Atlantic is altered. The meridional SST gradient anomaly is suggested to play some role in maintaining the SLP anomaly through changes in the near-surface baroclinicity and, hence, synoptic eddy activity. These results indicate that in addition to the remote influence from atmospheric teleconnections discussed in the previous studies, the local air–sea coupling in the South Atlantic also plays a role in the eastward propagation of SLP anomaly from the South Atlantic and, hence, the SLP variability in the southwestern Indian Ocean, which in turn causes decadal climate variability over southern Africa.

However, the relative importance of local and remote influences on the decadal climate variability over southern Africa remains uncertain. In observations taken over recent decades, the SST anomaly pattern associated with El Niño Modoki appears to generate an atmospheric teleconnection (e.g., Ratnam et al. 2014) in

Unauthenticated | Downloaded 05/18/25 08:50 PM UTC

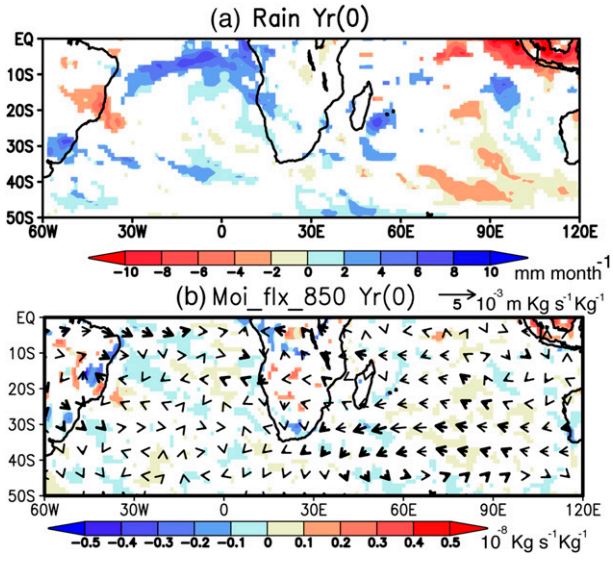

FIG. 14. (a) Composite rainfall anomalies during austral summer of Yr(0) in the CTR experiment. (b) As in (a), but for the moisture flux anomaly (arrows) and its divergence (color shading) at 850 hPa. Color shading and thick arrows indicate significant anomalies exceeding the 90% confidence level of the two-tailed Student's *t* test.

the South Pacific and South Atlantic [i.e., Pacific–South American (PSA) pattern], which may initiate the SLP and SST anomalies in the South Atlantic. The possible contribution from the low-frequency SST variability in the tropical Pacific was already suggested in previous studies (Mason and Jury 1997; Reason and Rouault 2002). On the other hand, the CGCM CTR experiment shows that the SLP anomaly in the southwestern Indian Ocean appears to have a strong association with the SAM. The possible link with the SAM has been recently discussed in the observational study of Malherbe et al. (2014). The relative importance of the SAM and the tropical Pacific SST variability cannot be easily derived from the current model experiments, because the SAM shows a significant relation to ENSO, especially during strong teleconnection season of austral summer (Pohl et al. 2010) and the tropical Pacific SST variability are likely to drive the SAM-like atmospheric anomalies in the Southern Hemisphere (Fogt and Bromwich 2006; L'Heureux and Thompson 2006).

Also, in the CGCM SAO experiment, the SLP anomaly appears in the southwestern Indian Ocean even without the SST anomaly in the South Atlantic. Hence, there is a possibility that a part of the low-frequency SST variability in the southern Indian Ocean might exist as internal variability of the basin's climate system. However, this does not explain the origin of the observed coupled variability in the South Atlantic. Therefore, further experiments would be required to identify the relative role of the remote and/or local impacts and internal climate variability in the decadal climate variability over southern Africa.

This study is the first to provide new evidence for the potential role of local air–sea coupling in the South Atlantic for the decadal climate variability over southern Africa. The accurate understanding of potential sources of decadal climate variability over southern Africa would be greatly helpful for improving the ability of model simulation and prediction for the long-term climate over southern Africa. This would benefit the local society to take preventative actions against the long-term climate-related risks. In this context, efforts in improving the model simulation and skillful prediction are under way.

Acknowledgments. The SINTEX-F2 was run on the Earth Simulator at the Japan Agency for Marine-Earth Science and Technology (JAMSTEC). Constructive comments from Drs. Toshio Yamagata, Yukio Masumoto, and Masami Nonaka helped improve the original manuscript. The authors are also grateful to three anonymous reviewers providing helpful comments to revise the manuscript. The present research is supported by JSPS KAKENHI Grant 15K17768, the Japan Science and Technology Agency/Japan Agency for Medical Research and Development through the Science and Technology Research Partnership for Sustainable Development (SATREPS), the Environment Research and Technology Development Fund (2-1405) of the Ministry of the Environment, Japan, and the Applied Centre for Climate and Earth System Studies (ACCESS) in South Africa.

REFERENCES

Adler, R. F., and Coauthors, 2003: The version-2 Global Precipitation Climatology Project (GPCP) monthly precipitation analysis (1979–present). *J. Hydrometeor.*, **4**, 1147–1167, doi:10.1175/1525-7541(2003)004<1147:TVGPCP>2.0.CO;2.

Allan, R. J., J. A. Lindesay, and C. J. Reason, 1995: Multidecadal variability in the climate system over the Indian Ocean region during the austral summer. *J. Climate*, **8**, 1853–1873, doi:10.1175/1520-0442(1995)008<1853:MVITCS>2.0.CO;2.

Ashok, K., S. K. Behera, S. A. Rao, H. Weng, and T. Yamagata, 2007: El Niño Modoki and its possible teleconnection. *J. Geophys. Res.*, **112**, C11007, doi:10.1029/2006JC003798.

Balmaseda, M. A., K. Mogensen, and A. T. Weaver, 2013: Evaluation of the ECMWF ocean reanalysis system ORAS4. *Quart. J. Roy. Meteor. Soc.*, **139**, 1132–1161, doi:10.1002/qj.2063.

Colberg, F., and C. J. C. Reason, 2007: Ocean model diagnosis of low-frequency climate variability in the South Atlantic region. *J. Climate*, **20**, 1016–1034, doi:10.1175/JCLI4055.1.

Cook, K. H., 2000: The South Indian convergence zone and interannual rainfall variability over southern Africa. *J. Climate*, **13**, 3789–3804, doi:10.1175/1520-0442(2000)013<3789:TSICZA>2.0.CO;2.

Unauthenticated | Downloaded 05/18/25 08:50 PM UTC

Dee, D. P., and Coauthors, 2011: The ERA-Interim reanalysis: Configuration and performance of the data assimilation system. *Quart. J. Roy. Meteor. Soc.*, **137**, 553–597, doi:10.1002/qj.828.

Ebita, A., and Coauthors, 2011: The Japanese 55-year Reanalysis "JRA-55": An interim report. *SOLA*, **7**, 149–152, doi:10.2151/sola.2011-038.

Engelbrecht, F. A., L. L. McGregor, and C. J. Engelbrecht, 2009: Dynamics of the conformal-cubic atmospheric model projected climate-change signal over southern Africa. *Int. J. Climatol.*, **29**, 1013–1033, doi:10.1002/joc.1742.

Fichefet, T., and M. A. Maqueda, 1997: Sensitivity of a global sea ice model to the treatment of ice thermodynamics and dynamics. *J. Geophys. Res.*, **102**, 12 609–12 646, doi:10.1029/97JC00480.

Fogt, R. L., and D. H. Bromwich, 2006: Decadal variability of the ENSO teleconnection to the high-latitude South Pacific governed by coupling with the southern annular mode. *J. Climate*, **19**, 979–997, doi:10.1175/JCLI3671.1.

Harris, I., P. D. Jones, T. J. Osborn, and D. H. Lister, 2014: Updated high-resolution grids of monthly climatic observations—The CRU TS3.10 Dataset. *Int. J. Climatol.*, **34**, 623–642, doi:10.1002/joc.3711.

Jury, M. R., 2015: Factors contributing to a decadal oscillation in South African rainfall. *Theor. Appl. Climatol.*, **120**, 227–237, doi:10.1007/s00704-014-1165-4.

——, B. Pathack, and B. J. Sohn, 1992: Spatial structure and interannual variability of summer convection over southern Africa and the SW Indian Ocean. *S. Afr. J. Sci.*, **88**, 275–280.

Kanamitsu, M., W. Ebisuzaki, J. Woollen, S. K. Yang, J. J. Hnilo, M. Fiorino, and G. L. Potter, 2002: NCEP–DOE AMIP-II Reanalysis (R-2). *Bull. Amer. Meteor. Soc.*, **83**, 1631–1643, doi:10.1175/BAMS-83-11-1631.

Kraus, E. B., and J. S. Turner, 1967: A one-dimensional model of the seasonal thermocline II. The general theory and its consequences. *Tellus*, **19A**, 98–106, doi:10.1111/j.2153-3490.1967.tb01462.x.

L'Heureux, M. L., and D. W. Thompson, 2006: Observed relationships between the El Niño–Southern Oscillation and the extratropical zonal-mean circulation. *J. Climate*, **19**, 276–287, doi:10.1175/JCLI3617.1.

Luo, J. J., S. Masson, S. K. Behera, P. Delecluse, S. Gualdi, A. Navarra, and T. Yamagata, 2003: South Pacific origin of the decadal ENSO-like variation as simulated by a coupled GCM. *Geophys. Res. Lett.*, **30**, 2250, doi:10.1029/2003GL018649.

——, ——, E. Roeckner, G. Madec, and T. Yamagata, 2005: Reducing climatology bias in an ocean–atmosphere CGCM with improved coupling physics. *J. Climate*, **18**, 2344–2360, doi:10.1175/JCLI3404.1.

Madec, G., 2008: NEMO ocean engine. Note du Pôle de Modélisation 27, ISSN 1288-1619, Institut Pierre-Simon Laplace (IPSL), France, 357 pp.

Malherbe, J., F. A. Engelbrecht, W. A. Landman, and C. J. Engelbrecht, 2012: Tropical systems from the southwest Indian Ocean making landfall over the Limpopo River Basin, southern Africa: A historical perspective. *Int. J. Climatol.*, **32**, 1018–1032, doi:10.1002/joc.2320.

——, W. A. Landman, and F. A. Engelbrecht, 2014: The bi-decadal rainfall cycle, Southern Annular Mode and tropical cyclones over the Limpopo River Basin, southern Africa. *Climate Dyn.*, **42**, 3121–3138, doi:10.1007/s00382-013-2027-y.

Mantua, N. J., S. R. Hare, Y. Zhang, J. M. Wallace, and R. C. Francis, 1997: A Pacific interdecadal climate oscillation with impacts on salmon production. *Bull. Amer. Meteor. Soc.*, **78**, 1069–1079, doi:10.1175/1520-0477(1997)078<1069:APICOW>2.0.CO;2.

Mason, S. J., 1990: Temporal variability of sea surface temperatures around southern Africa: A possible forcing mechanism for the 18-year rainfall oscillation. *S. Afr. J. Sci.*, **86**, 243–252.

——, and M. R. Jury, 1997: Climatic variability and change over southern Africa: A reflection on underlying processes. *Prog. Phys. Geogr.*, **21**, 23–50, doi:10.1177/030913339702100103.

Masson, S., P. Terray, G. Madec, J. J. Luo, T. Yamagata, and K. Takahashi, 2012: Impact of intra-daily SST variability on ENSO characteristics in a coupled model. *Climate Dyn.*, **39**, 681–707, doi:10.1007/s00382-011-1247-2.

Mo, K. C., and J. N. Paegle, 2001: The Pacific–South American modes and their downstream effects. *Int. J. Climatol.*, **21**, 1211–1229, doi:10.1002/joc.685.

Moisan, J. R., and P. P. Niiler, 1998: The seasonal heat budget of the North Pacific: Net heat flux and heat storage rates (1950–1990). *J. Phys. Oceanogr.*, **28**, 401–421, doi:10.1175/1520-0485(1998)028<0401:TSHBOT>2.0.CO;2.

Morioka, Y., K. Takaya, S. K. Behera, and Y. Masumoto, 2015: Local SST impacts on the summertime Mascarene high variability. *J. Climate*, **28**, 678–694, doi:10.1175/JCLI-D-14-00133.1.

Nakamura, H., and A. Shimpo, 2004: Seasonal variations in the Southern Hemisphere storm tracks and jet streams as revealed in a reanalysis dataset. *J. Climate*, **17**, 1828–1844, doi:10.1175/1520-0442(2004)017<1828:SVITSH>2.0.CO;2.

Nakamura, M., 2012: Impacts of SST anomalies in the Agulhas Current system on the regional climate variability. *J. Climate*, **25**, 1213–1229, doi:10.1175/JCLI-D-11-00088.1.

Ngara, T., D. L. McNaughton, and S. Lineham, 1983: Seasonal rainfall fluctuations in Zimbabwe. *Zimbabwe Agric. J.*, **80**, 149–150.

NOAA/ESRL/Physical Sciences Division, 2011: ICOADS 1 Degree, release 2.5, accessed 13 June 2015. [Available online at http://www.esrl.noaa.gov/psd/data/gridded/data.coads.1deg.html.]

North, G. R., T. L. Bell, R. F. Cahalan, and F. J. Moeng, 1982: Sampling errors in the estimation of empirical orthogonal functions. *Mon. Wea. Rev.*, **110**, 699–706, doi:10.1175/1520-0493(1982)110<0699:SEITEO>2.0.CO;2.

Paulson, C. A., and J. J. Simpson, 1977: Irradiance measurements in the upper ocean. *J. Phys. Oceanogr.*, **7**, 952–956, doi:10.1175/1520-0485(1977)007<0952:IMITUO>2.0.CO;2.

Pohl, B., N. Fauchereau, C. J. C. Reason, and M. Rouault, 2010: Relationships between the Antarctic Oscillation, the Madden–Julian oscillation, and ENSO, and consequences for rainfall analysis. *J. Climate*, **23**, 238–254, doi:10.1175/2009JCLI2443.1.

Power, S., T. Casey, C. Folland, A. Colman, and V. Mehta, 1999: Inter-decadal modulation of the impact of ENSO on Australia. *Climate Dyn.*, **15**, 319–324, doi:10.1007/s003820050284.

Qiu, B., and K. A. Kelly, 1993: Upper-ocean heat balance in the Kuroshio Extension region. *J. Phys. Oceanogr.*, **23**, 2027–2041, doi:10.1175/1520-0485(1993)023<2027:UOHBIT>2.0.CO;2.

Ratnam, J. V., S. K. Behera, Y. Masumoto, and T. Yamagata, 2014: Remote effects of El Niño and Modoki events on the austral summer precipitation of southern Africa. *J. Climate*, **27**, 3802–3815, doi:10.1175/JCLI-D-13-00431.1.

Reason, C. J. C., and C. R. Godfred-Spenning, 1998: SST variability in the South Indian Ocean and associated circulation and rainfall patterns over southern Africa. *Meteor. Atmos. Phys.*, **66**, 243–258, doi:10.1007/BF01026637.

——, and R. J. Murray, 2001: Modelling low frequency variability in Southern Hemisphere extra-tropical cyclone characteristics and its sensitivity to sea-surface temperature. *Int. J. Climatol.*, **21**, 249–267, doi:10.1002/joc.608.

Unauthenticated | Downloaded 05/18/25 08:50 PM UTC

——, and M. Rouault, 2002: ENSO-like decadal variability and South African rainfall. *Geophys. Res. Lett.*, **29**, doi:10.1029/2002GL014663.

——, R. J. Allan, and J. A. Lindesay, 1996: Evidence for the influence of remote forcing on interdecadal variability in the southern Indian Ocean. *J. Geophys. Res.*, **101**, 11 867–11 882, doi:10.1029/96JC00122.

——, C. R. Godfred-Spenning, R. J. Allan, and J. A. Lindesay, 1998: Air-sea interaction mechanisms and low-frequency climate variability in the south Indian Ocean region. *Int. J. Climatol.*, **18**, 391–405, doi:10.1002/(SICI)1097-0088(19980330)18:4<391::AID-JOC253>3.0.CO;2-C.

Reynolds, R. W., N. A. Rayner, T. M. Smith, D. C. Stokes, and W. Wang, 2002: An improved in situ and satellite SST analysis for climate. *J. Climate*, **15**, 1609–1625, doi:10.1175/1520-0442(2002)015<1609:AIISAS>2.0.CO;2.

Roeckner, E., and Coauthors, 2003: The atmospheric general circulation model ECHAM5: Part I: Model description. MPI-Rep. 349, Max-Planck-Institut für Meteorologie, Hamburg, Germany, 127 pp. [Available online at https://www.mpimet.mpg.de/fileadmin/publikationen/Reports/max_scirep_349.pdf.]

Schlesinger, M. E., and N. Ramankutty, 1994: An oscillation in the global climate system of period 65-70 years. *Nature*, **367**, 723–726, doi:10.1038/367723a0.

Schneider, U., A. Becker, P. Finger, A. Meyer-Christoffer, B. Rudolf, and M. Ziese, 2011: GPCC full data reanalysis version 6.0 at 0.5°: Monthly land-surface precipitation from rain-gauges built on GTS-based and historic data. Accessed 11 June 2015, doi:10.5676/DWD_GPCC/FD_M_V6_050.

Thompson, D. W. J., and J. M. Wallace, 2000: Annular modes in the extratropical circulation. Part I: Month-to-month variability. *J. Climate*, **13**, 1000–1016, doi:10.1175/1520-0442(2000)013<1000:AMITEC>2.0.CO;2.

Tyson, P. D., 1986: *Climatic Change and Variability in Southern Africa.* Oxford University Press, 220 pp.

——, T. G. Dyer, and M. N. Mametse, 1975: Secular changes in South African rainfall: 1880 to 1972. *Quart. J. Roy. Meteor. Soc.*, **101**, 817–833, doi:10.1002/qj.49710143008.

Valcke, S., A. Caubel, R. Vogelsang, and D. Declat, 2004: OASIS3 ocean atmosphere sea ice soil user's guide. Tech. Rep. TR/CMGC/04/68, CERFACS, Toulouse, France, 70 pp.

Venegas, S. A., L. A. Mysak, and D. N. Straub, 1997: Atmosphere–ocean coupled variability in the South Atlantic. *J. Climate*, **10**, 2904–2920, doi:10.1175/1520-0442(1997)010<2904:AOCVIT>2.0.CO;2.

Yasuda, I., T. Tozuka, M. Noto, and S. Kouketsu, 2000: Heat balance and regime shifts of the mixed layer in the Kuroshio Extension. *Prog. Oceanogr.*, **47**, 257–278, doi:10.1016/S0079-6611(00)00038-0.

Unauthenticated | Downloaded 05/18/25 08:50 PM UTC